# Experimental Characterization of the High Frequency Response of the LHO 4k IFO

## B: Parametric Conversion

LIGO-T030263-00-D

William E. Butler and Adrian C. Melissinos
*Department of Physics & Astronomy,*
*University of Rochester, Rochester NY. 14627*

November 24, 2003

# 1 Introduction

In part A [1] we examined the response of a single arm cavity to frequency sideband injection at multiples of 1/2 the free spectral range (FSR). Here we continue the IFO characterization by investigating the response of a single arm cavity as well as the response of the complete power recycled interferometer (PRIFO) to mirror motion. We use the term "parametric conversion" in the sense that harmonic variation ($\Omega$) of one parameter of the system (in this case the arm length) results in the conversion of a fraction of the carrier ($\omega$) to the sum and difference frequency ($\omega \pm \Omega$). For an optical cavity the effect can also be interpreted as arising from the Doppler shift of the carrier when reflected from a moving mirror. The conversion is most pronounced when the sidebands coincide with one of the resonant modes of the system. Since the modes of the IFO are equally spaced by the $f_{\rm fsr} = c/2L$, with $L$ the arm length, the parametric conversion response is peaked when $\Omega = 2\pi f_{\rm fsr}$. The width of the line is given by the $Q$ of the cavity (or the PRIFO). For a simple cavity:

$$Q = \frac{2L}{\lambda} F \simeq \frac{L}{\lambda} \frac{2\pi}{1 - r_A} = kL \frac{1}{1 - r_A}, \tag{1}$$

where $r_A$ is the (amplitude) reflectivity of the entrance mirror and we have ignored any losses, and $k = 2\pi/\lambda$. It follows that:

$$\Delta f = \frac{f_c}{Q} \simeq f_{\rm fsr} \frac{1 - r_A}{\pi}, \tag{2}$$

where $\Delta f$ is the FWHM power, or the FWHM at $1/\sqrt{2}$ of the fields.

The amplitude $E'$ of the parametrically converted signal is given on resonance by:

$$E' = 2 \times \frac{1}{2} h\, Q\, E_c\,, \tag{3}$$

where $E_c$ is the carrier amplitude and $h$ the fractional parametric perturbation. The additional factor of two is introduced because both the upper and lower sideband are populated. Eq(3) is valid for $hQ \ll 1$.

If the mirror position is given by:

$$x(t) = x_0 \cos(\Omega t),$$

then $h = x_0/L$. Introducing this expression for $h$ and the definition of $Q$ in Eq(3) we find (on resonance):

$$E' = E_c k x_0 \frac{2}{1 - r_A}. \tag{4}$$

Note that both fields $E_c$ and $E'$ are measured inside the cavity (at the mirror) but have different frequencies. To relate Eq(4) to the observed field we must propagate the incident carrier into the cavity as well as propagate the sideband $E'$ out of the cavity to the detection port. This is done using a matlab program written in-house using a matrix inversion method

of determining the fields of interest. This method was inspired by the approach taken by TWIDDLE [2], which is a mathematica program.

The same result is obtained by Regehr [3] and Lyons [4] who start from Eq(4) and propagate the fields analytically using the low frequency approximation. Since all results are valid modulo $f_{\rm fsr}$ the expressions given by Regehr and Lyons are equally applicable to the present case where $\Omega/2\pi \simeq f_{\rm fsr}$.

We also present some data on the response of the complete PRIFO to sideband injection.

# 2 Modulation and Demodulation

As in part A a first order expansion in the fields is sufficient and we still must treat the upper and lower sidebands separately. However, the modulation and resulting demodulation is slightly different in the case of mirror motion. This is because the r.f. sidebands are anti-resonant and do not enter the cavity. Thus they are not parametrically converted. With sideband injection there were 8 demodulation terms of interest: 4 terms with $f_{\pm rf}$ beating against $f_{\pm m}$ and 4 terms with $f_{\pm(rf\pm m)}$ beating against the carrier (where $f_{rf}$ indicates the non-resonant sideband required for heterodyne locking and $f_m$ indicates the sideband injected at the frequency of interest.) In the case of mirror motion only the 4 terms with$f_{\pm rf}$ beating against $f_{\pm m}$ are present where now $f_m$ is the mirror motion frequency.

One may be justly concerned about motion of the front mirror on which the r.f. is incident. This case can be analyzed by a thought experiment. Consider a simple two mirror cavity. Now consider that both mirrors are moving in a common motion, that is to say they are both oscillating sinusoidally at the same frequency and with the same phase so they both move in the same direction at the same time. The frequency response to this situation would be null, as the length of the cavity never changes leaving the resonance conditions static. Thus $E_m = 0$ and the sum of the terms $E_{\pm(rf\pm m)}$ is also 0 (as essentially $f_m = 0$ and the sum of $E_{\pm rf}$ is the locking signal which is null on resonance). Next consider moving only the back mirror. As the $f_{rf}$ is non-resonant there are no $E_{rf}$ sidebands incident on the moving mirror. Thus there can be no fields at frequency $f_{rf\pm m}$ so all fields $E_{\pm(rf\pm m)} = 0$. Finally consider moving only the front mirror. By superposition and comparison with the common mode motion of both mirrors we know that the sum of the fields at $f_{\pm(rf\pm m)}$ of the back mirror motion is equal in magnitude and negative in sign to the sum of the fields at $f_{\pm(rf\pm m)}$ of the front mirror motion. But these fields of the back mirror motion are zero so we can set all $E_{\pm(rf\pm m)} = 0$ in front mirror motion as well. It may be of interest to recall that resonance of the $E_{\pm(rf\pm m)}$ sidebands within the cavity gave rise to the $(1/2)f_{\rm fsr}$ features from sideband injection as demonstrated in part A. As such fields are zero with mirror motion we do not expect (nor do we see) any such features with mirror excitation.

With sideband injection the fields of interest for demodulation were of the form[1]

$$|E\ \{J_0(\Gamma_m) + J_1(\Gamma_m)e^{i\omega_m t} - J_1(\Gamma_m)e^{-i\omega_m t}\}\{J_0(\Gamma_s) + J_1(\Gamma_s)e^{i\omega_{\rm rf} t} - J_1(\Gamma_s)e^{-i\omega_{\rm rf} t}\}|^2,$$

[1]For pure phase modulation we again adopt the convention of the sidebands being real, the upper one positive and the lower one negative.

where $E$ is the unmodulated field. Adopting the notation that a subscript of 0 indicates the carrier field (the corresponding $e^{i\omega_c t}$ is left off as it conveniently cancels when evaluating the power as it is common to all terms; (r.f. and modulation frequencies are imposed relative to the carrier frequency), a subscript '$m$' indicates the applied modulation frequency, a subscript '$s$' indicates the non-resonant r.f. sidebands on the light necessary for locking the cavity by an optical heterodyning technique[5]. A subscript '$a$' indicates the sideband at the sum of the r.f. and modulation frequencies, and '$b$' indicates the sideband at the difference of the r.f. and modulation frequencies. It is also necessary to distinguish between the upper and lower sidebands as they obtain different phases upon reflection from the cavity (indicated by a '+' for the upper sideband and a '−' for the lower). Thus the signal is proportional to:

$$\mathrm{AS_{rf}} = \left| \begin{array}{c} E_0 + E_{m+}e^{i\omega_m t} - E_{m-}e^{-i\omega_m t} + E_{s+}e^{i\omega_s t} - E_{s-}e^{-i\omega_s t} \\ +E_{a+}e^{i(\omega_s+\omega_m)t} + E_{a-}e^{-i(\omega_s+\omega_m)t} - E_{b+}e^{i(\omega_s-\omega_m)t} - E_{b-}e^{-i(\omega_s-\omega_m)t} \end{array} \right|^2 . \quad (5)$$

Where all $E$-fields specified are the fields as they are incident on the diode at the port of interest. In the case of a single arm this is the reflection off the input mirror, in the case of the PRIFO it is the "dark" or "anti-symmetric" port. Equations for these fields are given in [6], or can be calculated by some other method (such as specified in section 3).

As we have just shown that the $f_{rf}$ and $f_m$ terms do not mix in the case of mirror excitation we simply use:

$$\mathrm{AS_{rf}} = \left| \; E_0 + E_{m+}e^{i\omega_m t} - E_{m-}e^{-i\omega_m t} + E_{s+}e^{i\omega_s t} - E_{s-}e^{-i\omega_s t} \; \right|^2 \quad (6)$$

For the demodulation signal we need only terms of the form $e^{\pm i(\omega_s \pm \omega_m)t}$. Thus we get:

$$\begin{array}{rl} \mathrm{AS_{rf}} = \cos(\omega_s t) & \left[ \begin{array}{c} e^{i\omega_m t}\left( E_{s-}E^*_{m-} + E_{m+}E^*_{s+} - E_{m+}E^*_{s-} - E_{s+}E^*_{m-} \right) \\ +e^{-i\omega_m t}\left( E_{s+}E^*_{m+} + E_{m-}E^*_{s-} - E_{m-}E^*_{s+} - E_{s-}E^*_{m+} \right) \end{array} \right] \\ -i\,\sin(\omega_s t) & \left[ \begin{array}{c} e^{i\omega_m t}\left( E_{s-}E^*_{m-} + E_{m+}E^*_{s+} + E_{m+}E^*_{s-} + E_{s+}E^*_{m-} \right) \\ -e^{-i\omega_m t}\left( E_{s+}E^*_{m+} + E_{m-}E^*_{s-} + E_{m-}E^*_{s+} + E_{s-}E^*_{m+} \right) \end{array} \right] \end{array} \quad (7)$$

We write Eq.(7) compactly as

$$\mathrm{AS_{rf}} = \cos(\omega_s t)[e^{i\omega_m t}\alpha' + e^{-i\omega_m t}\beta'] - i\,\sin(\omega_s t)[e^{i\omega_m t}\gamma' + e^{-i\omega_m t}\delta'] \quad (8)$$

where we substitute $\alpha'$, $\beta'$, $\gamma'$ and $\delta'$ for the corresponding sets of field terms. Upon closer inspection of Eq.(7) it is apparent that $\beta' = \alpha'^*$ and $\delta' = \gamma'^*$, so that Eq.(8) can be further simplified to

$$\begin{array}{rcl} \mathrm{AS_{rf}} & = & \cos(\omega_s t)[\alpha' e^{i\omega_m t} + (\alpha' e^{i\omega_m t})^*] - i\,\sin(\omega_s t)[\gamma' e^{i\omega_m t} - (\gamma' e^{i\omega_m t})^*] \\ & = & 2\cos(\omega_s t)\Re e\{\alpha' e^{i\omega_m t}\} - 2\sin(\omega_s t)\Re e\{i\gamma' e^{i\omega_m t}\} \end{array} \quad (9)$$

Since we have adopted the convention of the sidebands being real, we imply that the r.f. sidebands were imposed by a *sine* modulation. If we had adopted the convention of

imaginary sidebands it would imply *cosine* modulation. Thus in our convention in-line demodulation selects the term oscillating as $\sin(\omega_s t)$ while quadrature demodulation selects the term oscillating as $\cos(\omega_s t)$. Cosine modulation would reverse which term is selected by in-line vs. quadrature demodulation, however it would also change $\alpha'$ and $\gamma'$ such that regardless of the convention, in-line (or quadrature) signals are convention independent. If we assume a phase difference $\phi$ between the demodulating r.f and the r.f. component of the detected signal we find:

$$\begin{aligned} \text{AS\_I}(\phi) &= \Re e\{(-i\gamma' \cos\phi + \alpha' \sin\phi) e^{i\omega_m t}\} \\ \text{AS\_Q}(\phi) &= \Re e\{(\alpha' \cos\phi + i\gamma' \sin\phi) e^{i\omega_m t}\} \end{aligned} \tag{10}$$

The LIGO convention for modulation and resulting demodulation is to use cosine modulation [3, 5]. Nominally the fact that we are using a different convention should not cause any problems with readout of the signals from the IFO as the in-line signal is the same regardless of convention as is the quadrature signal. It did however, cause a certain amount of confusion as the readouts being used (I$mon$ and Q$mon$) were analog monitoring points located on the demod board and once they were digitized their phase was adjusted by 90 degrees, thus making I$mon$ = Q, and Q$mon$ = I. However, it also appears that in the formulation of the LIGO demodulation theory the distance from the recycling mirror (RM) to the beam-splitter (BS) was not taken into account. And as that distance is approximately 1/4 of the wavelength of the r.f. sidebands it has the effect of switching the r.f. modulation convention. All this has no effect upon the operation of the IFO as in practice the signal is routed to the demod board and the phase is tuned until one of the channels provides a maximum for the signal. This channel is then defined as the channel of interest. The effect upon fitting routines can be summarized as follows: In single-arm mode, I$mon$ = Q and Q$mon$ = I, In PRIFO mode, I$mon$ = I and Q$mon$ = Q.

# 3 Field Calculation Methods

Two separate methods are used to model the IFO output. The first method is through algebraic calculation and the use of the formulae given in [6]. This was used to fit the sideband injection into the IFO as the computational requirements of this method are significantly smaller. This also allows a point of comparison with results obtained from the second method. The second method was through a matrix inversion process similar to that done in TWIDDLE [2]. The primary reason for using the matrix method of calculation is that some of the symmetry arguments used to obtain the formulae for the first method do not hold when shaking a single mirror. Although a single mirror excitation could theoretically be done by the superposition of a common and a differential shake (both of which have sufficient symmetry to be adapted to the formulae in [6]) the matrix method is well adapted to computer calculation.

Both simulation methods required an additional parameter to properly simulate a locked PRIFO using the conventions adopted earlier. In [6] the fields returning from the arms (Eqs.

9 and 10) are given by:

$$\frac{E_D}{E_{in}} = it_{bs}r_y r_{bs}e^{-i\frac{\omega}{c}2l_y} + ir_{bs}r_x t_{bs}e^{-i\frac{\omega}{c}2l_x} \quad (11)$$

$$\frac{E_r}{E_{in}} = r_{bs}r_y r_{bs}e^{-i\frac{\omega}{c}2l_y} - t_{bs}r_x t_{bs}e^{-i\frac{\omega}{c}2l_x} \quad (12)$$

which eventually lead to (Eq. 12) the dark port output:

$$\frac{E_D}{E_0} = \frac{(-t_{rm})(t_{bs}r_y r_{bs}e^{-i\frac{\omega}{c}2l_y} + r_{bs}r_x t_{bs}e^{-i\frac{\omega}{c}2l_x})e^{i\frac{\omega}{c}l_{in}}}{1 - r_{rm}(r_{bs}r_y r_{bs}e^{-i\frac{\omega}{c}2l_y} - t_{bs}r_x t_{bs}e^{-i\frac{\omega}{c}2l_x})} \quad (13)$$

Now the standard calculational procedure involves setting the carrier frequency to zero and using modulation frequencies relative to the carrier. Although this method worked fine with no adjustments for the simple cavity calculations it can be seen from Eqs.(11 & 12) that when this is done the "dark" port has a field magnitude $\simeq 2$ while the "refl" port has a field magnitude $\simeq 0$. When the full carrier frequency is used then the length values of $l_x$ and $l_y$ can be set such that the "dark" port is sufficiently dark. As this led to an over-sensitivity of the simulation to some of the lengths the equations were modified to establish proper resonance conditions with relative frequencies. Also a parameter $\xi$ was introduced to allow easy modification of the resonance condition. This leads to the modified equations:

$$\frac{E_D}{E_{in}} = -it_{bs}r_y r_{bs}e^{-i\frac{\omega}{c}2l_y}e^{i\xi} + ir_{bs}r_x t_{bs}e^{-i\frac{\omega}{c}2l_x}e^{-i\xi} \quad (14)$$

$$\frac{E_r}{E_{in}} = -r_{bs}r_y r_{bs}e^{-i\frac{\omega}{c}2l_y}e^{i\xi} - t_{bs}r_x t_{bs}e^{-i\frac{\omega}{c}2l_x}d^{-i\xi} \quad (15)$$

$$\frac{E_D}{E_0} = \frac{(-t_{rm})(-t_{bs}r_y r_{bs}e^{-i\frac{\omega}{c}2l_y}e^{i\xi} + r_{bs}r_x t_{bs}e^{-i\frac{\omega}{c}2l_x}e^{-i\xi})e^{i\frac{\omega}{c}l_{in}}}{1 - r_{rm}(-r_{bs}r_y r_{bs}e^{-i\frac{\omega}{c}2l_y}e^{i\xi} - t_{bs}r_x t_{bs}e^{-i\frac{\omega}{c}2l_x}e^{-i\xi})} \quad (16)$$

The nominal value is $\xi = 0$ to establish resonance conditions at zero frequency. In order to better fit the data $\xi$ is varied off nominal, allowing us to determine how well the IFO is tuned.

The second method used to model the data is a matrix inversion calculation. Each location near an optic within the system is given a number to denote the electric field at that location. This includes the fields incident on the optic and those fields leaving the optic in all directions of interest. Then the relative field equations are set out in a matrix form. For example for an optic with fields incident from both sides (like the input mass for a simple cavity) we can label the field incident from the left as 1, the field leaving to the left as 2, the field leaving to the right as 3 and the field incident from the right as 4, as illustrated in Fig.(1). Now we say that field 1 is equal to itself and leave it at that. We then say field 2 is itself plus field 1 times the optic's reflectivity plus field 4 times the optic's transmissivity. Field 3 is itself plus field 4 times the reflectivity and field 1 times the transmissivity. Field 4 is itself plus likely another field with a spatial propagation term. Next we write the set of linear equations so that they are all equal to zero (or in the case of field 1 equal to 1).

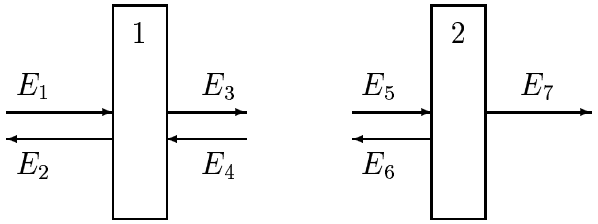


Figure 1: Simple Fabry-Perot Cavity

Then write it in matrix form so that the element $(j,k)$ refers to the contribution of field $k$ to the field $j$. In our simple example here (1,1) = 1, (2,2) = 1, (2,1) = $-r_1$, (2,4) = $-it_1$. This gives us a matrix, which when multiplied by a column vector of the field values gives a column vector of [1,0,0,0,...]. Thus when the matrix (M) is inverted we can multiply it by the injection vector [1,0,0,0,...] and get a vector of the fields in the system at all locations. It is also possible to modify the injection vector to simulate injection of sidebands at a different location, for example by shaking a mirror instead of sideband injection on the incident field.

We show an example in Fig.(1) and the accompanying Eqs.(17,18). The $\phi_l$ in the equations is the length propagator to appropriately adjust the phase and is given by $\phi_l = \omega l/c$ where $l$ is the length of the cavity. Given that the matrix is frequency dependent, when implemented in matlab a 3-dimensional matrix is used so that a 2-dimensional matrix is available for each frequency of interest.

$$\begin{bmatrix} 1 & 0 & 0 & 0 & 0 & 0 & 0 \\ -r_1 & 1 & 0 & -it_1 & 0 & 0 & 0 \\ -it_1 & 0 & 1 & -r_1 & 0 & 0 & 0 \\ 0 & 0 & 0 & 1 & 0 & -e^{-i\phi_l} & 0 \\ 0 & 0 & -e^{-i\phi_l} & 0 & 1 & 0 & 0 \\ 0 & 0 & 0 & 0 & -r_2 & 1 & 0 \\ 0 & 0 & 0 & 0 & -it_2 & 0 & 1 \end{bmatrix} \times \begin{bmatrix} E_1 \\ E_2 \\ E_3 \\ E_4 \\ E_5 \\ E_6 \\ E_7 \end{bmatrix} = \begin{bmatrix} 1 \\ 0 \\ 0 \\ 0 \\ 0 \\ 0 \\ 0 \end{bmatrix} \tag{17}$$

$$\begin{bmatrix} E_1 \\ E_2 \\ E_3 \\ E_4 \\ E_5 \\ E_6 \\ E_7 \end{bmatrix} = \begin{bmatrix} 1 & 0 & 0 & 0 & 0 & 0 & 0 \\ -r_1 & 1 & 0 & -it_1 & 0 & 0 & 0 \\ -it_1 & 0 & 1 & -r_1 & 0 & 0 & 0 \\ 0 & 0 & 0 & 1 & 0 & -e^{-i\phi_l} & 0 \\ 0 & 0 & -e^{-i\phi_l} & 0 & 1 & 0 & 0 \\ 0 & 0 & 0 & 0 & -r_2 & 1 & 0 \\ 0 & 0 & 0 & 0 & -it_2 & 0 & 1 \end{bmatrix}^{-1} \times \begin{bmatrix} 1 \\ 0 \\ 0 \\ 0 \\ 0 \\ 0 \\ 0 \end{bmatrix} \tag{18}$$

# 4 Data Fits

We have fitted the following data sets:

(a) Single arm excitation of ITMX (Data obtained in October 2002; Figure 2)

(b) PRIFO excitation of ITMX (Data obtained in October 2002; Figure 3)

(c) PRIFO excitation of ITMX (Data obtained in December 2002; Figure 4); Both Q-phase and I-phase are shown.

(d) Figure 5 is an enlarged view of the I-phase data and fit of Figure 4

(e) Figure 6 is an enlarged view of the Q-phase data and fit of Figure 4.

(f) PRIFO Sideband Injection (Data obtained in October 2002); Q-phase (Figure 7) and I-phase (Figure 8) were recorded.

Case (a) is simple to fit either algebraically or with the matrix method. The parameters varied were the normalization, demodulation phase and a frequency independent noise level (which is also multiplied by the normalization factor). The fit is shown in Fig.2 and it returned the following values:

$$\begin{aligned} N &= 3.42 \times 10^{-9} \\ \phi &= 0^{\mathrm{o}} \\ A_{\mathrm{noise}} &= 2.06 \times 10^{-8} \end{aligned}$$

Note that the noise level is essentially zero. The noise parameter was a remnant of the fits to sideband injection [1] where the parameter was very important for the fit. The arm length was kept fixed at 3995.05948 m as determined previously [1]. The data is cut off at 37.75 kHz due to the presence of a strong internal resonance of the test mass at 37.8 kHz. This may also be the reason that the data does not agree better with the fitted curve.

Data on the full Power Recycled Interferometer (PRIFO) was taken primarily in two distinct periods. As extensive commissioning work was constantly in progress on the IFO at this time there is a distinct difference in the instrument response. Primarily this can be understood as a decrease in the amount that $\xi$ (as defined in Sec. 3) varied off the "perfect" dark port condition. It is believed that all other parameters that would affect the fit stayed essentially constant during this period. The $\xi$ parameter can vary from measurement to measurement as it is an artifact of the quality of feedback. Thus if the control loop is already near its limit, then a small increase in the ambient noise, although not necessarily enough to cause a loss of lock, would result in a decrease of the lock quality (an increase in $\xi$) and not an increase in the feedback signal.

With the complete PRIFO many more parameters have to be specified. These are given in Table 1 and were obtained from a combination of design specifications, measured values and best fits as indicated. With the complete PRIFO the data exhibits the broad resonance apparent when a single arm is excited (Fig 2) referred to as the "cavity pole", and an additional much narrower peak referred to as the "double cavity pole". This arises because the recycling mirror significantly improves the finesse of the common mode signal. However, the common mode signal can not appear at the AS port except for a small leakage that arises because of the "asymmetry" between the two arms. This asymmetry is introduced in order

| Parameter | Value | |
|---|---|---|
| Laser Power in TE00 Mode | 1 | (W) |
| Resonant SB frequency* | 24481323 | (Hz) |
| Resonant SB modulation depth | 0.45 | |
| Distance RM to BS† | 3 | (m) |
| Distance BS to in-line ITM‡ | 6.191 - asym | (m) |
| Distance BS to off-line ITM‡ | 6.191 + asym | (m) |
| Michelson Asymmetry (asym)‡ | 0.151 | (m) |
| Michelson Asymmetry (asym)§ | 0.110 | (m) |
| Distance in-line Arm* | 3995.05948 | (m) |
| Distance off-line Arm* | 3995.01332 | (m) |
| BS Reflectance¶ | 0.49997999 | |
| BS Transmittance¶ | 0.49997999 | |
| BS Loss¶ | 40e-6 | |
| RM Reflectance¶ | 0.971825 | |
| RM Transmittance¶ | 0.0281 | |
| RM Loss¶ | 75e-6 | |
| ITM Reflectance¶ | 0.971825 | |
| ITM Transmittance¶ | 0.0281 | |
| ITM Loss¶ | 75e-6 | |
| ETM Reflectance¶ | 0.999925 | |
| ETM Transmittance¶ | 5e-6 | |
| ETM Loss¶ | 70e-6 | |
| ITM / ETM pendulum frequency‖ | 0.74 | (Hz) |

*Obtained from fits in [1].

†Estimate based on experience on-site.

‡Obtained from [7].

§Obtained from fits presented in this paper.

¶Values are Power coefficients, for amplitude coefficients take the square root. Values obtained from specifications [8] and previously designed simulations for the E2E program [9, 10].

‖Obtained from [11].

Table 1: Nominal Parameters for WA 4k Interferometer

to provide maximal r.f. sideband power at the AS port. When the PRIFO is not perfectly locked ($\xi \neq 0$) the common mode signal becomes more pronounced at the AS port. This is the case in Fig. 3.

Moving a mirror in one arm is equivalent to the presence of both a differential mode and a common mode signal as the excitation of a single ITM is equivalent to a linear combination of common and differential motion of both ITMs. That is, by changing the length of a single arm one changes both the average length of the two arm cavities as well as the difference between the lengths of the two arm cavities. Now the PRIFO is designed so as to have the anti-symmetric (AS) port on a common motion "dark fringe" and a differential motion "bright fringe". Thus common motion of the arm cavities will not result in a signal (this is because a properly polarized gravitational wave excites the differential motion of the test masses). As far as the differential signal is concerned there is no recycling mirror, the light simply leaves the arm cavity and exits to the AS port diode. A differential motion signal from the PRIFO is the same as that from a single arm. A common motion signal however, is sent back to the recycling mirror and is reflected back to the arm cavities. This has the effect of increasing the reflectivity of the respective arm cavity's input mirror; thus giving it a higher finesse and a more narrow frequency response. The common mode appears as a narrow peak or "glitch" superimposed on the differential mode broad signal. Fig. 3 shows the data obtained in October 2002 with the complete PRIFO and the corresponding fit. The parameters are:

$$\begin{aligned} N &= 0.46 \times 10^{-6} \\ \phi &= 0^{o} \qquad \text{(specified, not fit)} \\ A_{\text{noise}} &= -0.32 \\ \xi &= 4.00^{o} \end{aligned}$$

Fig. 4 shows the data obtained in December 2002 with the complete PRIFO and the corresponding fit to the I phase. The *same parameters* were then used for the Q phase prediction:

$$\begin{aligned} N &= 2.82 \times 10^{-6} \\ \phi &= 0^{o} \qquad \text{(specified, not fit)} \\ \xi &= 6.82^{o} \\ \text{Mich Asymmetry} &= 0.21 \text{ meters} \\ \text{Distance off} - \text{line Arm} &= 3995.01112 \text{ meters} \end{aligned}$$

The agreement in this case is quite encouraging. Expanded views of these curves are shown in Figs 5, 6. Fig 5 shows the I-phase theory and its corresponding fit, while Fig 6 shows the Q-phase theory and the Q-phase prediction using the parameters obtained in the I-phase fit. As a significant amount of work had taken place on the instrument between the measurements leading to values in Table 1 and the time these measurements were taken, some of the parameters in the Table were modified. As independent measurements to determine these

changed parameters were not taken at this time, and this fit uses several inter-dependent parameters, these parameters are not said to have been measured. This does, however, demonstrate a minimum level at which the data can be fit to theory.

Finally Figs. 7 and 8 show sideband injection with the complete PRIFO. The fit to the Q-phase (Fig 7) is satisfactory and returned the following parameters:

$$\begin{aligned} N &= 7.08 \times 10^{-3} \\ A_{\text{noise}} &= 0.12 \\ \xi &= 4.16^{\text{o}} \end{aligned}$$

Note that the resonant peak has a FWHM of $\simeq$ 2Hz as expected for the double cavity pole. Incidentally this corresponds to a Q-value $\nu/\Delta\nu = 1.5 \times 10^{14}$! One may also have observed that the normalization value is significantly larger than that for the single arm measurement. This is due to the fact that for the single arm measurement the light must be transmitted through both the recycling mirror and the beam-splitter (without resonating) before encountering the arm cavity, while the simulation starts at the arm cavity with no input attenuation. For the PRIFO the experiment and the simulation start at a much more equivalent input level.

The fit for the I-phase returns different parameters. Both the $\xi$ term and the normalization are different.

$$\begin{aligned} N &= 15.13 \times 10^{-3} \\ A_{\text{noise}} &= 0.01 \\ \xi &= 2.50^{\text{o}} \end{aligned}$$

This can be understood in part because the signal is very noisy. However, the mirror excitation measurement (Fig. 3) taken within a few minutes of the sideband injection measurements was reasonably fit with similar parameters. Thus we conclude that sideband injection with the full PRIFO is much more sensitive to the fit parameters. This was verified by our modeling.

# 5 Calibration and Normalization

In these measurements ITMX was driven at frequencies around $f_{\text{fsr}} = 37.52$ kHz. This was rather unusual (since in normal IFO operations only frequencies up to a few kHz are used to calibrate the instrument response) and was achieved by introducing a modified controller which could drive the test mass coils at high current. To relate the drive signal to mirror motion we use the D.C. calibration values:

| | |
|---|---|
| 0.163 | nm / count drive[2] |
| 20,000 / 175 | counts / $\text{mV}_{\text{pp}}$ on coils |

[2]Obtained from the calibration group at LHO [12].

22 / .2 $\quad$ $\mathrm{mV_{pp}}$ on coils / $\mathrm{V_{pp}}$ drive[3]

Thus at DC (0.1 Hz) the calibration is:

$$x_{\mathrm{DC}} = 2.049\ \mu\mathrm{m}\ /\ \mathrm{V_{pp}}\ \mathrm{drive} \tag{19}$$

To obtain the calibration at $f = f_{\mathrm{fsr}} = 37.52$ kHz we treat the optic as a simple pendulum driven far off resonance [13]:

$$x(f) = \frac{x_{\mathrm{DC}}}{\sqrt{[1-(\frac{f}{f_0})^2]^2 + (\frac{1}{Q}\frac{f}{f_0})^2}}. \tag{20}$$

Here $f_0$ is the resonant frequency of the pendulum mode $f_0 = 0.743$ Hz [11] and $Q$ the Q-value. For $f/f_0 \gg 1$, Eq(20) reduces to:

$$x(f) \simeq x_{\mathrm{DC}} \left(\frac{f_0}{f}\right)^2. \tag{21}$$

Therefore we take the calibration at $f_{\mathrm{fsr}} = 37.52$ kHz of

$$x(37.52\ \mathrm{kHz}) = 8.04 \times 10^{-16}\ \mathrm{m}\ /\ \mathrm{V_{pp}}\ \mathrm{drive}. \tag{22}$$

Next we must establish the relation between the optical power (at the harmonic that is demodulated) and the signal recorded on the SRS spectrum analyzer. These factors are shown in Table 2 below and consist of: (a) Signal attenuation by an E/O Shutter, (b) A series of pick-offs (as the LIGO design calls for an eventual set of four photodiodes at the AS port), (c) The photodiode conversion efficiency, (d) The photodiode r.f. impedance and (e) The signal transmission efficiency from r.f. output to the demodulated output. Thus 1 W

| Parameter | Value | |
|---|---|---|
| E/O Shutter | 7 | % |
| Beam-path | 0.245 | |
| Diode Eff. | 0.64 | A / W |
| Diode Imped. | 4000 | Ω |
| Signal Transfer | 0.269 | $V_{pk}$ (SRS) / $V_{pk}$ signal |
| Total | 11.76 | $V_{pk}$ (SRS) / W |

Table 2: Output Attenuation

of optical power yields 11.76 V on the SRS spectrum analyzer or:

$$11.76\ \mathrm{V}\ /\ \mathrm{W}. \tag{23}$$

[3]Measured differential between the drive sent to the optic and the amount seen by the optic.

Finally to compare our model to the data we must relate the field $E_0$ in the arm to the input laser power (including the recycling effects). We must also know the r.f. sideband field at the AS port. We initially will assume an input power $I_{\rm in} = 1$ W.

The PRM (power) build-up factor is determined as follows: with the recycling mirror misaligned the intensity through a single locked arm is measured. The measurement is repeated with the PRIFO locked and the ratio of the transmitted intensities is designated as NPTR (the Normalized Power TRansmitted through the arm cavity).

$$NPTR = \frac{I_{\rm in}\,\frac{1}{2}\,B_{\rm PRM}B_X T_X}{I_{\rm in}\,\frac{1}{2}\,T_{\rm RM}B_X T_X} = \frac{B_{\rm PRM}}{T_{\rm RM}} \tag{24}$$

where $B_X$ and $B_{\rm PRM}$ are the build up factors in the arm and the recycling cavity, $T_X$ and $T_{\rm RM}$ the (power) transmission coefficients of the arm end mirror and of the recycling mirror.

The field in the arm is given by:

$$E_X = E_{\rm incident}\sqrt{B_X} = \sqrt{I_{\rm in}\,\frac{1}{2}\,B_{\rm PRM}B_X} \tag{25}$$

The measured value of NPTR was 1400 and $T_{\rm RM} = 0.03$ and therefore $B_{\rm PRM} = 42$. For $B_X$ we can use:

$$\frac{t_{\rm ITM}^2}{(1 - r_{\rm ITM}r_{\rm ETM})^2} = 139. \tag{26}$$

Thus for $I_{\rm in} = 1$ W:

$$E_X = 54\ (\mathrm{W}^{\frac{1}{2}}) \tag{27}$$

The modulation index during this period was $\Gamma = 0.45$, so that

$$J_0(\Gamma) = 0.95 \quad J_1(\Gamma) = 0.22$$

Therefore the carrier field of Eq(27) must be multiplied by 0.95 and the sideband field at the AS port is:

$$E_S = 0.22\ (\mathrm{W}^{\frac{1}{2}}) \tag{28}$$

In our numerical program, the term driving the audio sideband:

$$xkE_0 \tag{29}$$

was set to unity, as was the r.f. sideband field. Here $k$ is the carrier wave vector:

$$k = \frac{2\pi}{\lambda_{\rm light}} = 5.91 \times 10^6 \tag{30}$$

Using the results of Eqs(22,30,27 and 28) the output of the program must be multiplied by:

$$(8.04 \times 10^{-16})(5.91 \times 10^6)(54 \times 0.95)(0.22) = 5.36 \times 10^{-8} \tag{31}$$

to give the optical power at the demodulation harmonic. Finally multiplying by the factor of Eq(23) we obtain the normalization that leads to signal voltage:

$$N = 6.30 \times 10^{-7} \tag{32}$$

Eq(32) is valid for 1 V drive and 1 W input.

We compare this normalization with the data of Fig. 4. Since the data gives the transfer function, it already assumes 1 V drive. The input power was estimated at 0.9 W[4] so that the calculated normalization factor should be:

$$N = 5.68 \times 10^{-7} \tag{33}$$

The observed normalization instead is:

$$N = 2.82 \times 10^{-6} \tag{34}$$

In view of the uncertainty in the mirror motion given in Eq(22) due to nearby test mass resonances and the long extrapolation in Eq(21) the factor of four between the calculated and observed values is acceptable. We also stress that the same normalization is used for both the ASQ and ASI quadratures.

# 6 Sensitivity Limits

So far we have shown "transfer functions" obtained by sweeping the frequency of the ITM excitations, or of the injected sideband around $f_{\rm fsr}$. To establish the sensitivity of the PRIFO to a G.W. (i.e. a parametric perturbation) we drive the ITM at a fixed frequency and record the FFT at the AS port. This is shown in Figure 9 where the ITM was driven at $f_{\rm fsr}$, and the AS_I quadrature was monitored.

We note that the signal and noise levels are

$$V_S = 87\ \mu\text{V} \quad V_N = 40\ \text{nV}$$

This signal level is in agreement with that displayed in Fig 4. The bandwidth of the data acquisition was 50 Hz / (800 channels) = 0.0625 Hz so that the noise spectral density

$$S_N = 0.16\ \mu\text{V}/\sqrt{\text{Hz}}$$

This noise level is in agreement with other measurements and corroborated by [14]. When the E/O shutter was closed from 7% to 3% the noise density decreased further to $S_N = 0.11\ \mu\text{V}/\sqrt{\text{Hz}}$, an indication that not all the noise was from the electronics.

The signal responds linearly to the ITM drive as shown in Fig. 10 for both quadratures. We therefore assume that we can extrapolate to very small drive values being limited only

[4] As per elog entry 11/25/2002 by Nergis & PeterF

by the noise floor. Since 1 V drive corresponds to $x_0 = 8 \times 10^{-16}$ m drive, the strain in the arm is $h = x_0/L = 2 \times 10^{-19}$ for 1 V drive. Assuming optimal orientation of the G.W., both arms will contribute. Thus signal to noise unity (S/N = 1) is reached when

$$h = 1.8 \times 10^{-22} \ /\sqrt{\text{Hz}} \tag{35}$$

This level of strain can therefore be achieved in a single measurement with BW = 1 Hz. Excluding DAQ overhead 86,400 such measurements can be averaged in a day, reducing the noise fluctuations so that S/N = 1 is reached for

$$h = 6 \times 10^{-25} \ /\sqrt{\text{Hz}} \tag{36}$$

This low value for the strain is valid only at $f_{\text{fsr}}$ and falls off as the frequency is shifted from the resonant value. However thermal noise in the test masses will probably raise the noise floor above this limit.

If the G.W. signal is continuous, in frequency, as is the case for the stochastic background, the response will have the typical shape of Fig. 4. Averaging over the direction of incidence and polarization for the stochastic background reduces the sensitivity by a factor of 5.3 as calculated by D.Sigg [15].

# References


[1] William E. Butler and Adrian C. Melissinos. Experimental Characterization of the High Frequency Responce of the LHO 4k IFO, A: Sideband Injection. Technical report, University of Rochester, Dept. of Physics & Astronomy, 2003. LIGO Internal #: T030163.

[2] Martin W. Regehr, James E. Mason, and Hiro Yamamoto. Twiddle (ver. 3.0) a program for analyzing interferometer frequency response (mathematica 3.0). Technical report, Caltech, February 1999. LIGO Internal #: T990022.

[3] Martin W. Regehr. *Signal Extraction and Control for an Interferometric Gravitational Wave Detector*. PhD thesis, California Institute of Technology, 1995.

[4] Torrey T. Lyons. *An Optically Recombined Laser Interferometer for Gravitational Wave Detection*. PhD thesis, California Institute of Technology, 1997.

[5] ISC team. Length sensing & control subsystem final design. Technical report, Caltech, July 1998. LIGO Internal #: T980068.

[6] William E. Butler. Field calculations for a power recycled michelson interferometer with fabry-perot arms, a first principles approach. Technical report, University of Rochester, Dept. of Physics & Astronomy, May 2001. LIGO Internal #: T030162.

[7] Dennis Coyne. Recycling cavity layout. Technical report, Caltech, 1997. LIGO Internal #: D970003.

[8] G. Billingsley, B. Kells, H. Yamamoto, J. Camp, D. Li, H. Armandula, S. Bell, and S. Elieson. Core optics components final design. Technical report, Caltech, April 1998. LIGO Internal #: E980061.

[9] Biplab Bhawal, Matt Evans, Edward Maros, Malik Rahman, and Hiro Yamamoto. Physics of end-to-end model. Technical report, LIGO Technical Report #: T970196, November 1997.

[10] Biplab Bhawal, Matt Evans, Edward Maros, Malik Rahman, and Hiro Yamamoto. Overview of end-to-end model. Technical report, LIGO Internal #: T970193, November 1997.

[11] Michael Landry and David Ottaway. Summary of mechanical resonances in the LIGO hanford interferometers. Technical report, LIGO Internal #: T000020, March 2000.

[12] Michael Landry, Luca Matone, Benoit Mours, and Peter Shawhan. E2 calibration study of the Hanford 2km IFO. Technical report, LIGO Internal #: T000115, October 2000.

[13] Leonard Meirovitch. *Elements of Vibration Analysis*. McGraw-Hill Book Company.

[14] R. Savage and M. Rakhmanov. Study of cavity field dynamics at high frequencies with the H1 interferometer. LSC Meeting, Livingston, LA, March 2003. LIGO Internal #:G030058.

[15] Daniel Sigg. Strain calibrations in LIGO. Technical report, LHO Hanford, March 1993. LIGO Internal #: T970101.

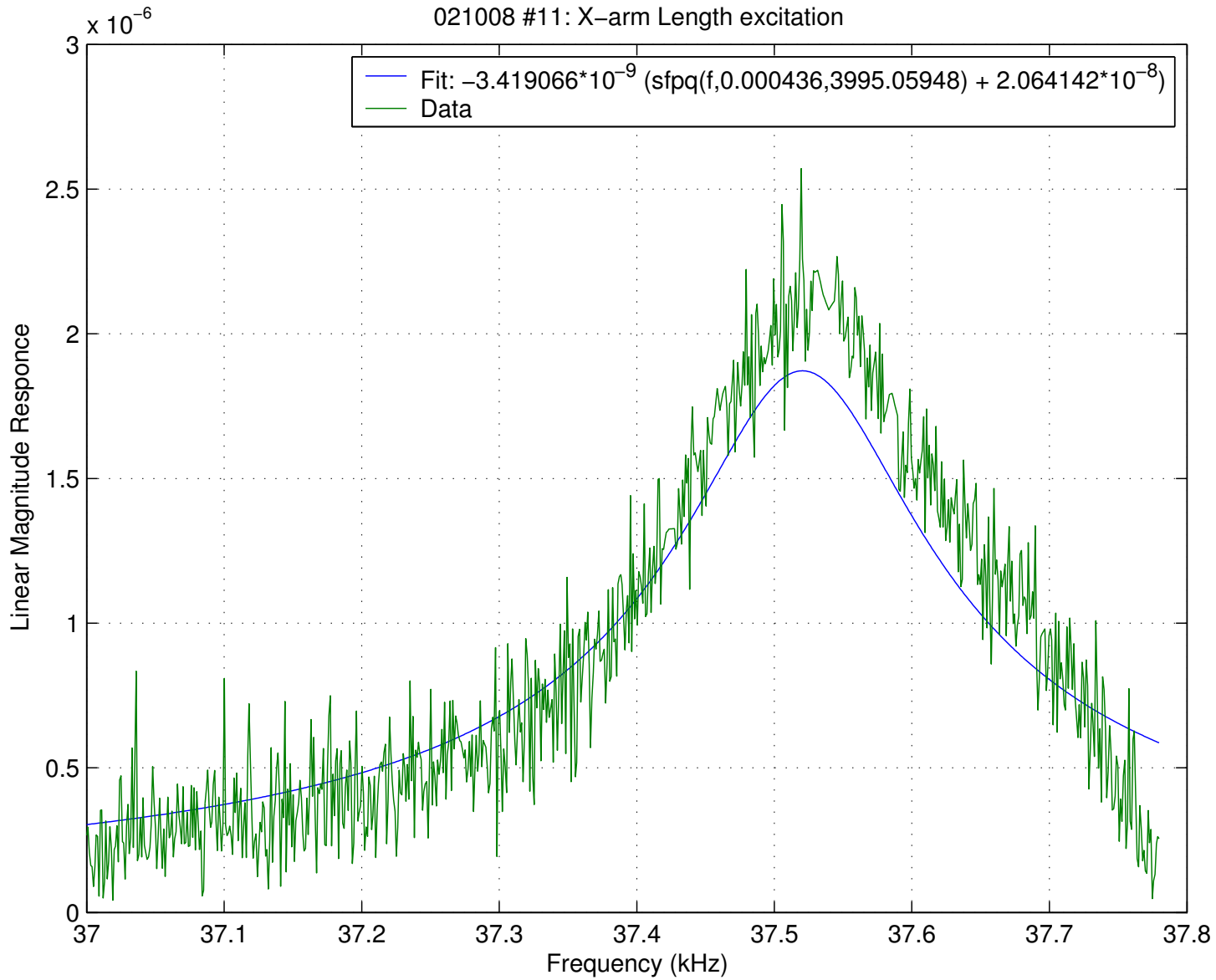


Figure 2: X-arm Shake Response

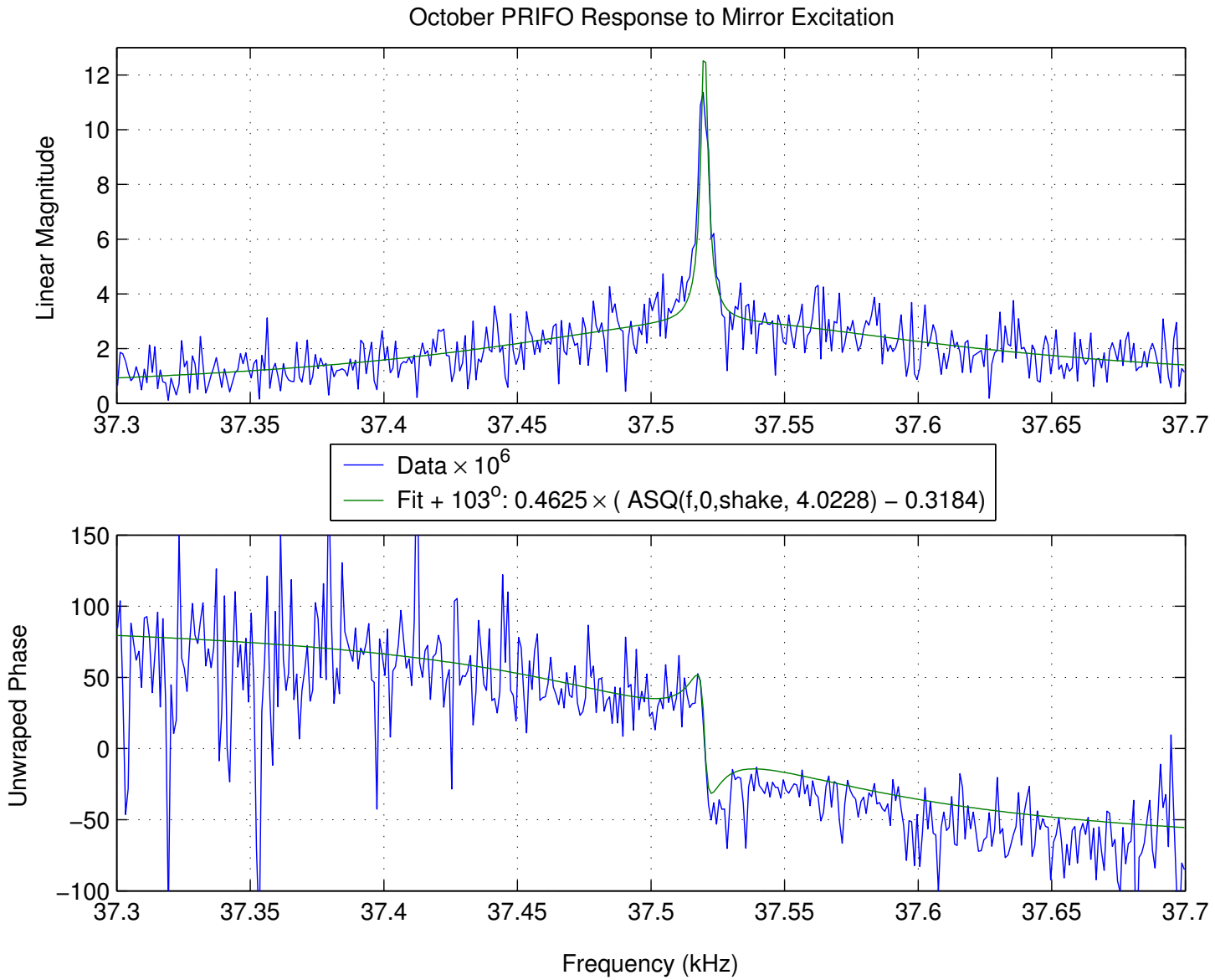


Figure 3: Full-IFO Mirror Excitation Response, Q-phase October

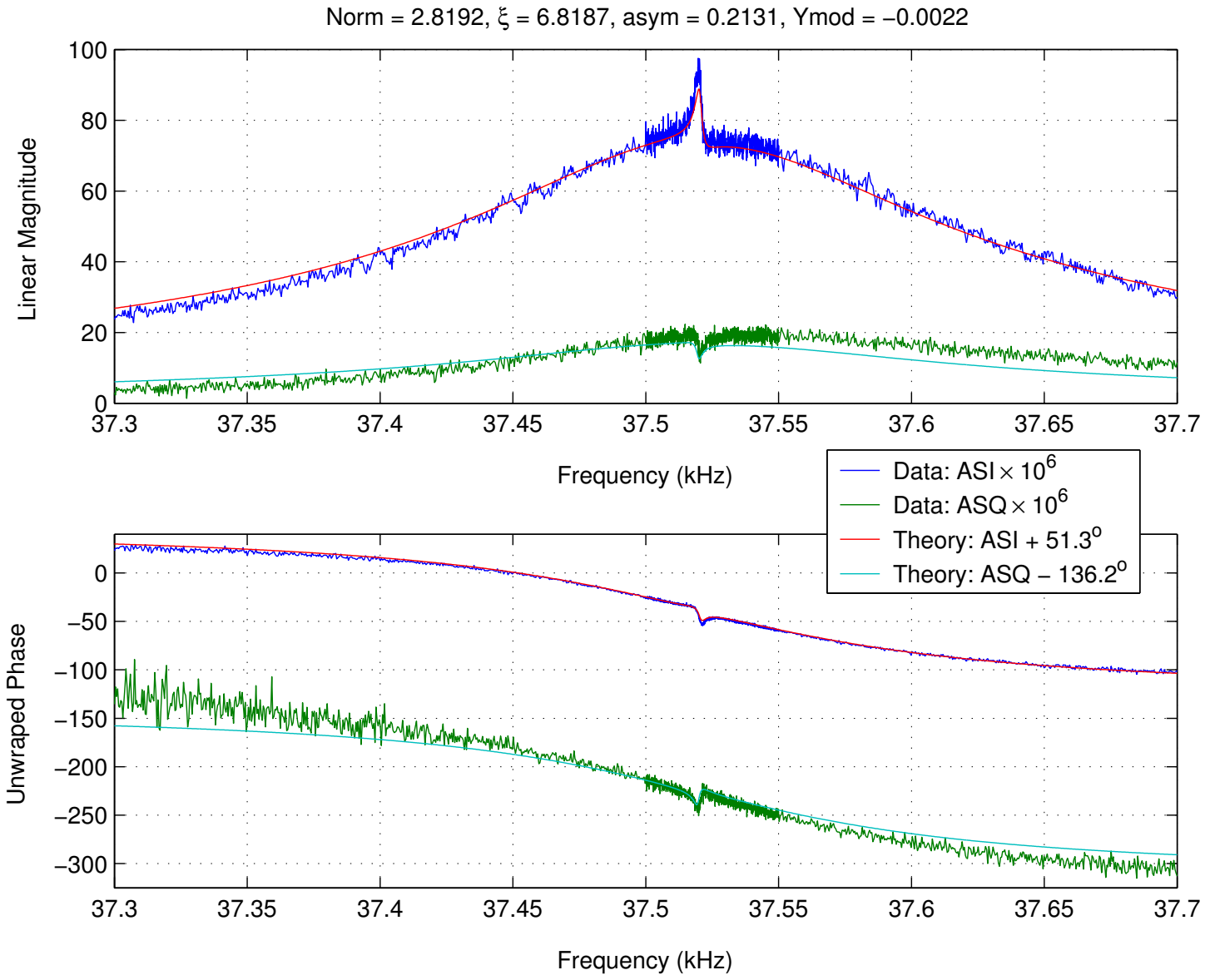


Figure 4: Full-IFO Mirror Excitation Response, I and Q phase

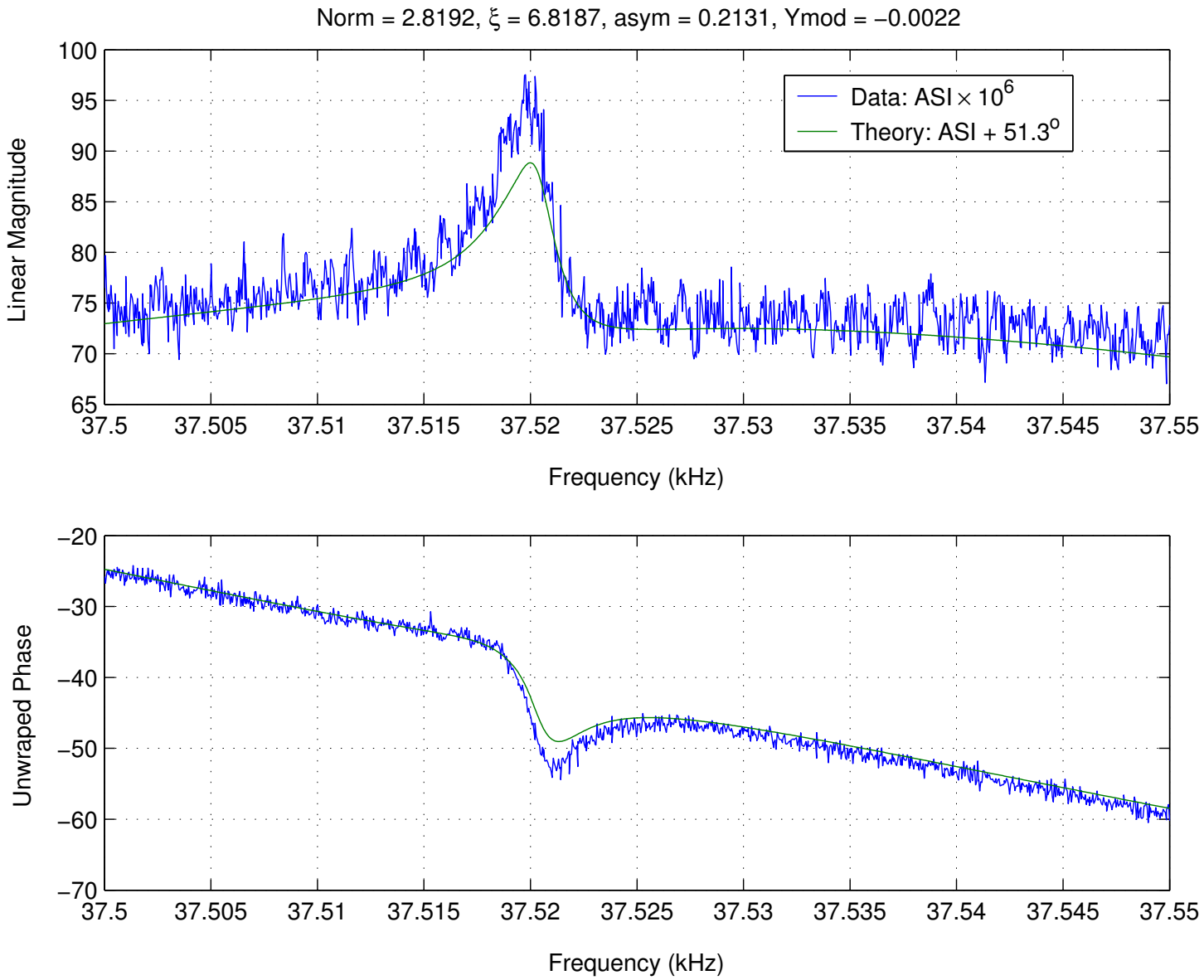


Figure 5: Full-IFO Mirror Excitation Response, I-phase

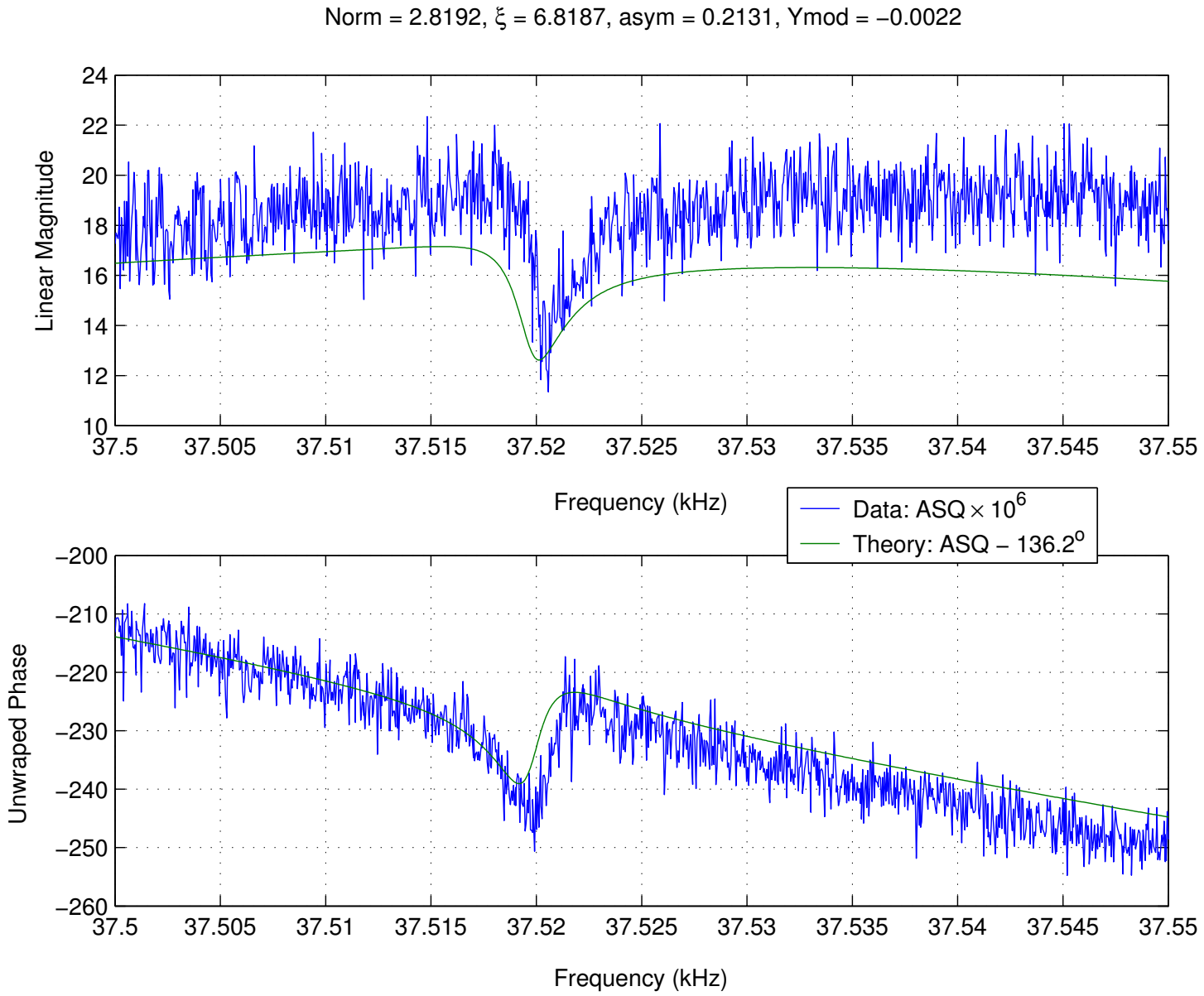


Figure 6: Full-IFO Mirror Excitation Response, Q-phase

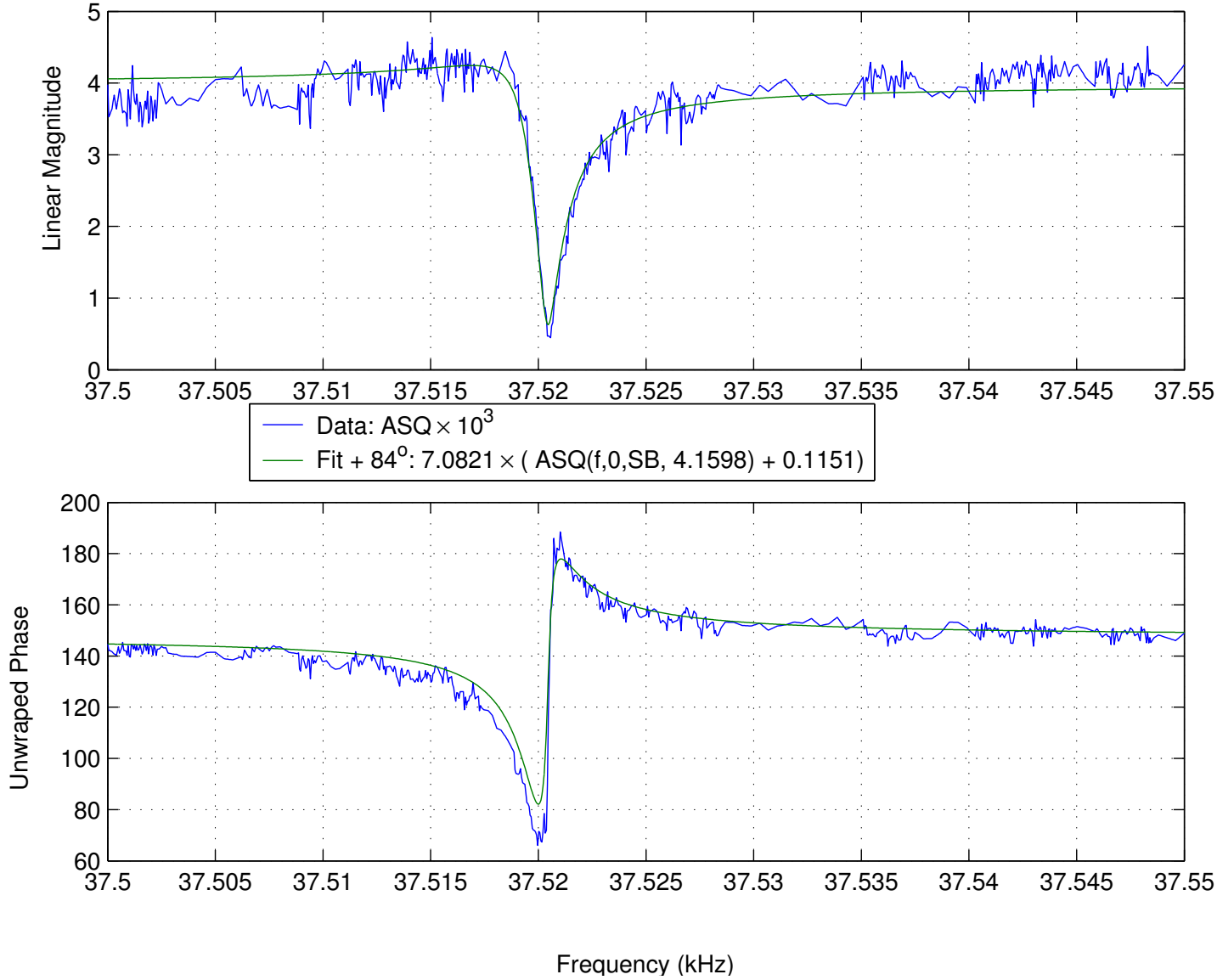


Figure 7: Full-IFO Sideband Injection Response, Q-phase

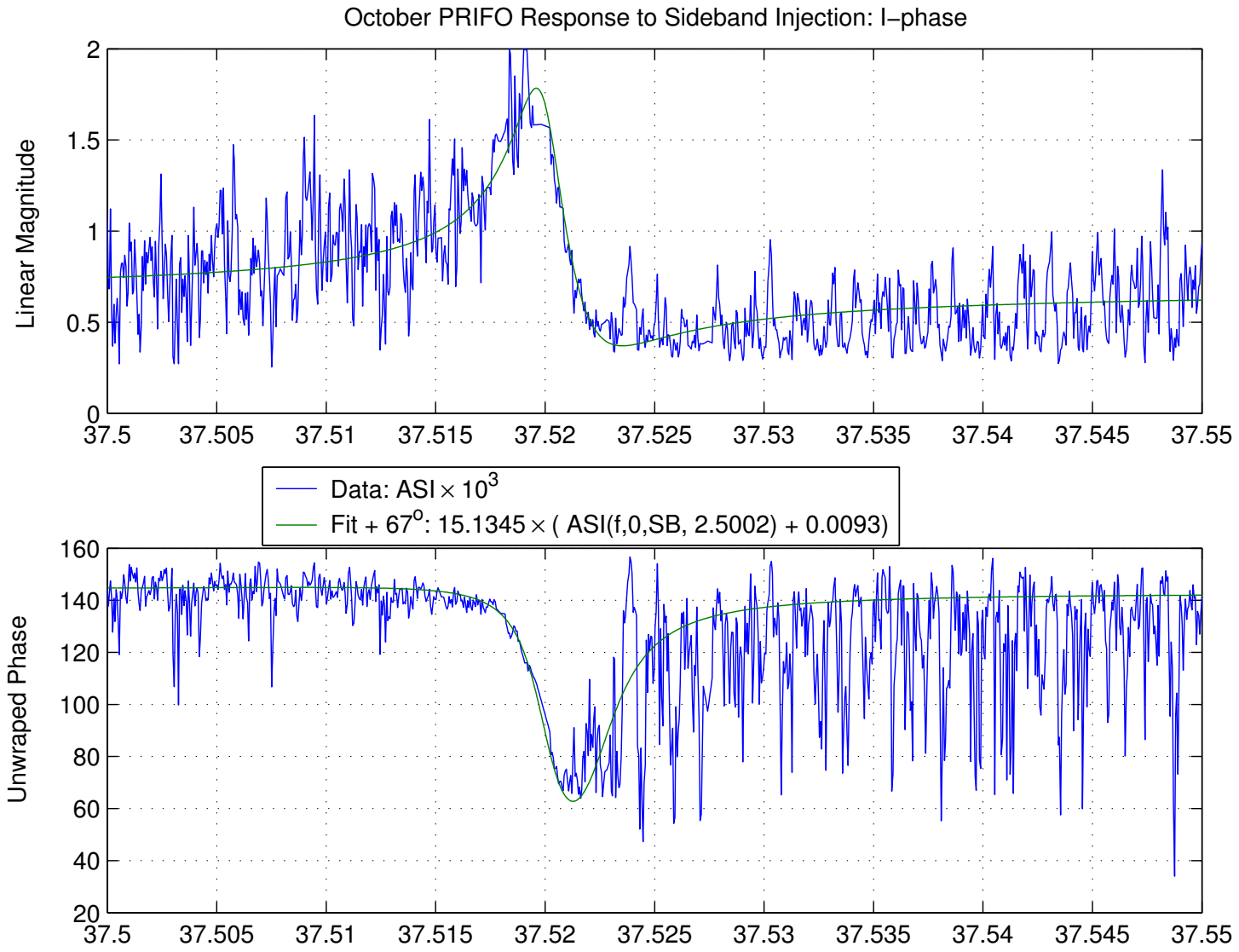


Figure 8: Full-IFO Sideband Injection Response, I-phase

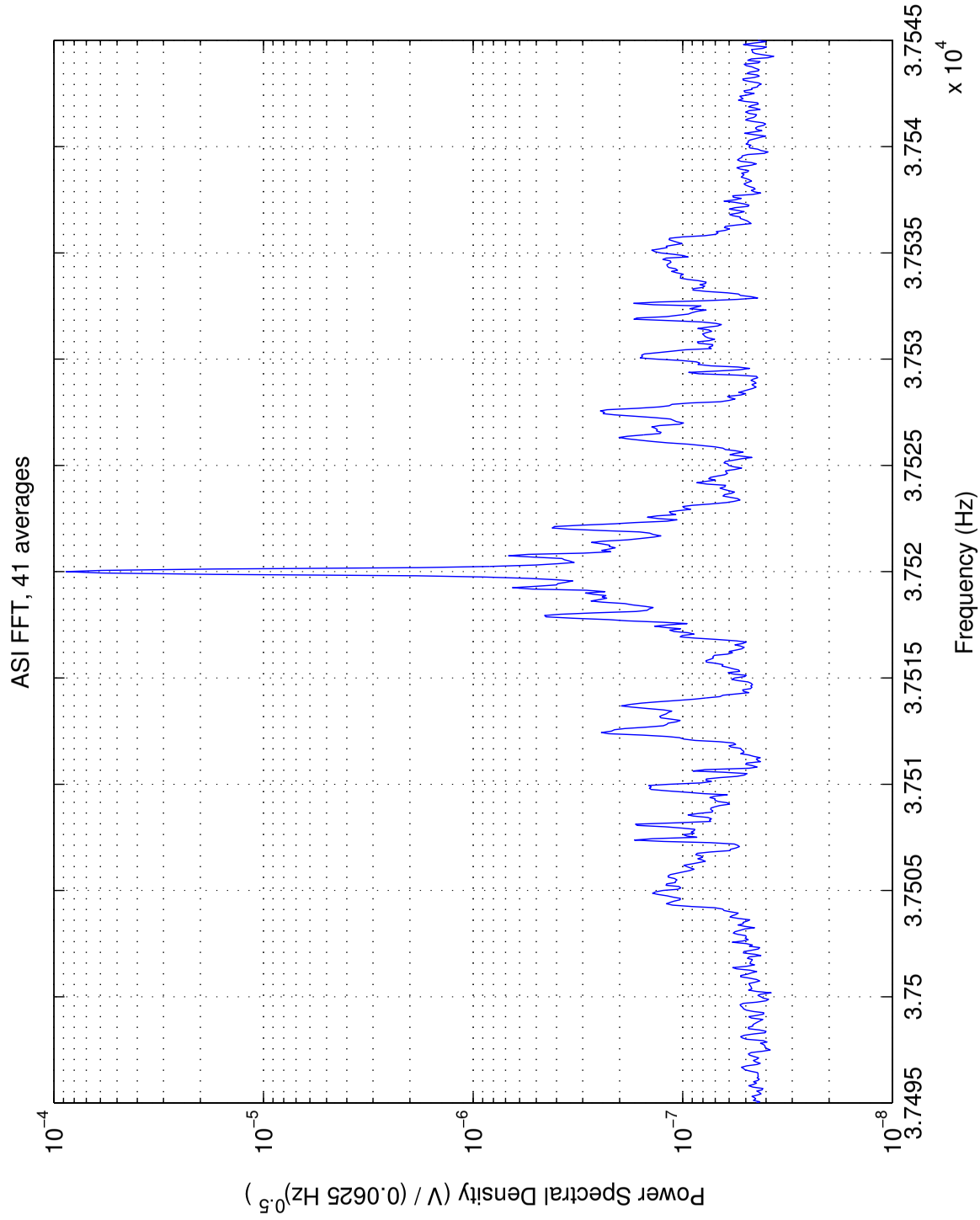


Figure 9: FFT of AS_I with mass excitation of $1V_{pk}$ @ 37.52 kHz

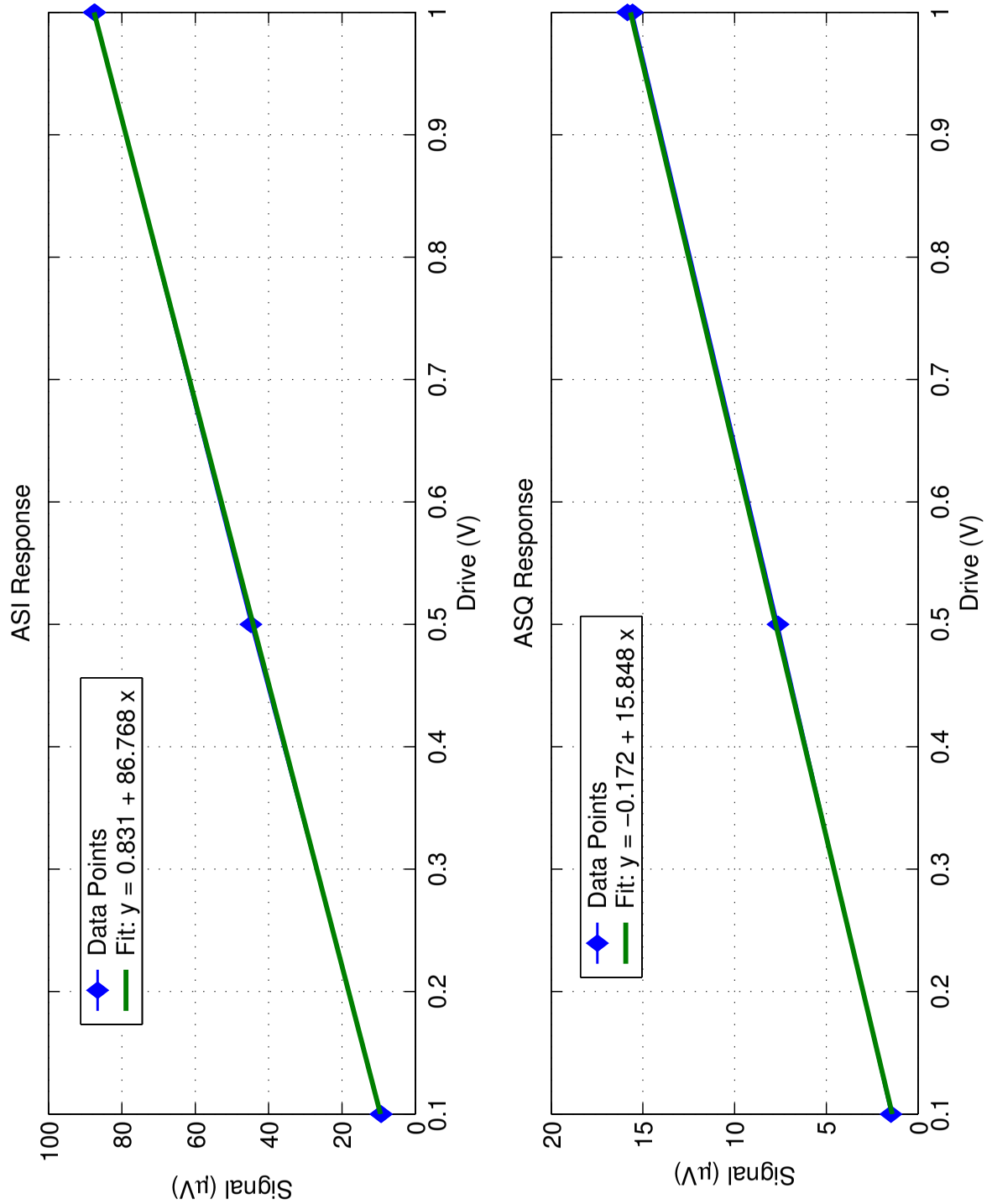


Figure 10: Response of the IFO to ITM excitation at varying magnitudes in both I and Q quadratures.